




Transmission Characteristics of Terahertz Imaging Detection in Smoke Environments

Dan Zhang , School of Building Environment Engineering, Zhengzhou University of Light Industry, Zhengzhou, China and Henan Engineering Research Center for Intelligent Buildings and Human Settlements, Zhengzhou, China

Jingchao Qu and Yintao Ouyang, School of Building Environment Engineering, Zhengzhou University of Light Industry, Zhengzhou, China

Sen Li* and Yinmao Song, School of Building Environment Engineering, Zhengzhou University of Light Industry, Zhengzhou, China and Henan Engineering Research Center for Intelligent Buildings and Human Settlements, Zhengzhou, China

Received: 18 August 2021/**Accepted:** 9 March 2022/**Published online:** 23 March 2022

Abstract. The terahertz imaging detection technology is applied to low-visibility fire environments to improve the traditional imaging detection equipment affected by the changes in the morphology and particle size distribution of smoke particles. This study focus on the transmission characteristics of terahertz waves in fire and smoke environments. A model for the propagation of terahertz waves is obtained. Terahertz imaging equipment is used to experimentally investigate the flue gas environment generated by three standard fires and combined with numerical simulations to analyze the influence of the terahertz wave transmission under different flue gas environments. The results show that the transmission of terahertz waves in a flue gas environment is affected by factors such as the smoke particle size and flue gas concentration; however, the transmission is significantly better than that obtained with traditional detection methods. In standard fire experiments, the terahertz equipment can achieve good imaging results, and the transmittance of terahertz waves is maintained above 88%.

Keywords: Terahertz waves, Fire smoke particles, Image detection, Transmission characteristics

1. Introductions

In a fire environment, the large amount of dense smoke produced by an incomplete combustion can cause harm to the human body and reduce visibility, rendering a familiar environment unrecognizable [1]. Therefore, one of the key technologies in the field of fire safety is the detection of people and objects in low-visibility fire environments [2], which helps firefighters to quickly locate trapped people and organize rescue. In recent years, the fire environment imaging technol-

*Correspondence should be addressed to: Sen Li, E-mail: lisen@zzuli.edu.cn



ogy has become a new research topic in the field of fire detection [3]; however, certain existing imaging detection approaches such as visible light and infrared thermal imaging, are affected by the concentration of smoke and temperature [4, 5]. Their impact is significant, leading to deviations in the test results. Terahertz (THz) waves are electromagnetic waves with a frequency of 0.1 THz–10 THz, located between microwave and infrared waves [6], it takes into account the permeability and high spatial resolution. The THz imaging and spectroscopy technology is used in radars, communications, medical imaging, security inspection, and agriculture [7–9]; however, no systematic research has been carried out on the influence of fire smoke environments on the propagation characteristics of terahertz waves.

Relevant studies have shown that electromagnetic waves with frequencies above 100 GHz are affected by the flue gas environment. The morphological characteristics, particle size and concentration of the smoke particles in the flue gas environment cause various degrees of attenuation of electromagnetic waves [10, 11]. Therefore, to study the transmission of terahertz waves in an environment with fire smoke particles, it is necessary to consider the morphological characteristics of smoke particles and the attenuation characteristics of the terahertz wave transmission caused by the dynamic changes in the size distribution of smoke particles. In the early studies on the transmission characteristics of electromagnetic waves in granular media, the granular medium was first regarded as spherical [12], and it was then found that the nonspherical particle model is more consistent with the medium morphology existing in the atmosphere [13–15]. The scattering characteristics of smoke particles are significantly stronger than those of biological aerosols [16], so the introduction of a fractal condensate structure to treat fire smoke particles has increased the accuracy of the analysis of the electromagnetic wave transmission characteristics in fire smoke particles. Different incident light wavelengths will have different performances in a smoke environment. When the incident light wavelength is equivalent to the smoke particle size, the light is greatly affected by the smoke particle morphology and particle size distribution; when the incident light wavelength is much larger than the smoke particle size, the smoke particles can be described approximately as spherical particles [17]. This provides a theoretical support for studying the propagation characteristics of terahertz waves with wavelengths (30 μm –3 mm) longer than visible light in a smoke environment.

Several researchers have compared the transmission of terahertz waves with infrared, laser and other millimeter waves in smoke and aerosol particle environments [18, 19], laying a foundation for the further study of the transmission characteristics of terahertz waves in fire and smoke environments. Ken et al. developed an active fire imaging system based on terahertz electromagnetic waves and compared them with visible light and infrared imaging. It can be seen from the experimental results that compared with visible light and infrared imaging, the terahertz object image obtained in the simulated fire smoke environment is clearer, and the signal-to-noise ratio of the infrared image decreases with the increase in the extinction coefficient. Infrared imaging cannot be clearly imaged in a thick smoke environment [20]. This study presents the propagation characteristics of terahertz waves in a flue gas environment and an investigation of the attenuation character-

istics of smoke particles to terahertz waves. A terahertz passive imaging system is employed for the measurements, i.e., collecting the image data in a simulated fire environment, to analyze the transmission characteristics of terahertz waves in the smoke environment with numerical simulations, and to obtain the transmission model of terahertz waves in the smoke environment.

2. Materials and Methods

Optical flue gas measurements and terahertz imaging detection are used simultaneously, in order for the detection results to have the same time scale. The experimental results are verified by numerical simulation methods, and the radiation transfer equation is used as a simulation analysis model. Furthermore, the influence of the smoke particle size and smoke concentration changes on the transmission of terahertz waves is determined, and a theoretical model for the transmission of terahertz waves in a smoke environment is established.

2.1. Simulation Models and Methods

2.1.1. Single particle model and simulation method. Figure 1a shows polyurethane fire smoke particles collected by a high-resolution field emission scanning electron microscope [21, 22]. Fire smoke particles are not spherical, but are an aggregation of different numbers of elementary particles, and their shape can be described by Eq. (1) [23].

$$N_f = k_f \left(\frac{R_g}{d_p} \right)^{D_f} \quad (1)$$

In the equation, R_g represents the radius of gyration of the aggregate; N_f represents the number of elementary particles in the aggregate; d_p represents the diameter of the elementary particles; k_f is a pre-factor; D_f represents the fractal dimension. The smoke particle agglomerate simulation generator is used to establish the smoke particle types in the agglomerate structure according to Eq. (1). The parameters are set as follow: $N = 100$, $D_f = 1.8$, and $k_f = 2.3$.

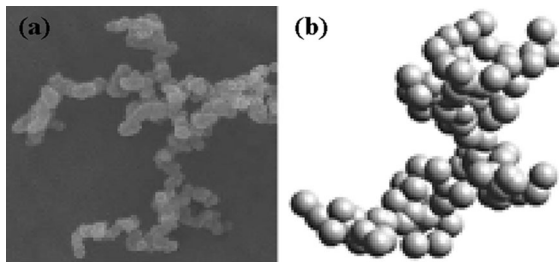


Figure 1. a SEM scanning of smoke particles and b Simulation of the smoke generation.

The light scattering of terahertz waves by nonspherical smoke particles can be described using the Stokes vector. The corresponding incident and outgoing light transmission equations are shown in Eq. (2) [24], where I represents the light intensity, and Q , U , and V represent other light wave parameters. For the polarization state, the right side of the equation represents the incident parameter, and the left side of the equation represents the exit parameter [25]. The light scattering Muller matrix can be represented by the 4×4 order matrix on the right side of the equation, $\{S_{ij}(\theta)(i,j = 1,2,3,4)\}$, where each element represents the light scattering characteristics. $S_{11}(\theta)$ describes the energy transfer between incident and scattered light, while the other elements represent the transfer characteristics of polarized light at different incident angles.

$$\begin{bmatrix} I_{sca}(\theta) \\ Q_{sca}(\theta) \\ U_{sca}(\theta) \\ V_{sca}(\theta) \end{bmatrix} = \begin{bmatrix} S_{11}(\theta) & S_{12}(\theta) & 0 & 0 \\ S_{21}(\theta) & S_{22}(\theta) & 0 & 0 \\ 0 & 0 & S_{33}(\theta) & S_{34}(\theta) \\ 0 & 0 & -S_{34}(\theta) & S_{44}(\theta) \end{bmatrix} \times \begin{bmatrix} \theta \\ Q_i(\theta) \\ U_i(\theta) \\ V_i(\theta) \end{bmatrix} \quad (2)$$

Since smoke particles possess a unique fractal aggregate structure, the discrete dipole approximation (DDA) method is employed to simulate the scattering and absorption characteristics of a single smoke particle and to calculate the extinction characteristics of non-spherical particles [26]. The DDA algorithm is a commonly used numerical method for studying the absorption and scattering of aerosols, dust particles, etc. The DDA algorithm uses an array of a large number of dipoles to model particles of any shape, and obtains the absorption and scattering characteristics of the object by solving the polarization of the dipoles under the irradiation of incident electromagnetic waves [27]. In this study, the DDSCAT 7.3 version of the DDA algorithm related software is used to calculate the absorption and scattering characteristics of terahertz waves for a single smoke particle [28].

When using the DDA method, it is first necessary to determine the effective radius and shape of the smoke particles as well as the size and coordinates of the particles that constitute smoke particles. It is also required to determine the complex refractive index of the smoke particles in different terahertz wave bands. In order to ensure accuracy when calculating the absorption and scattering characteristics of the smoke particles, the input model must satisfy Eq. (3) [29].

$$|m'|k\lambda d < 0.5, \quad k\lambda = 2\pi/\lambda \quad (3)$$

where m' is the complex refractive index and d (μm) is the distance between two adjacent dipoles. Among these parameters, the wavelength λ (μm) and the complex refractive index m' are candidates for investigating. To satisfy the above Eq. (3), d needs to be sufficiently small, that is, the number of dipoles N should be sufficiently large to describe the morphological characteristics of the smoke particles.

2.1.2. Smoke Particle Group Model and Simulation Method Tam et al. proposed the radiative transfer equation in 1982 to replace the Lambert Beer law to solve the output light power. This approach effectively overcame the drawbacks of the Lambert Beer law, disregarding the effect of light scattering on transmission [30, 31]. When light is transmitted in a flue gas environment, the smoke particles impede light transmission through absorption and scattering. Light absorption does not affect the transmission direction; however, the scattering of light causes it to diffuse and change direction. The light that changed direction reaches other particles, where it is absorbed and scattered again, leading to multiple scattering effects. The multi-scattering effect increases the intensity of the incident light and affects the calculation of the output light power. The radiative transfer equation is shown in Eq. (4) [32]. The influence of the multiple scattering effect is considered in the light transmission calculation, improving its accuracy.

$$\mu \frac{dI(\tau, \mu, \varphi)}{d\tau} = I(\tau, \mu, \varphi) - S(\tau, \mu, \varphi) \quad (4)$$

The three-dimensional reference coordinates of the transmission equation are shown in Fig. 2. In Eq. (4) [32], I is the output light power and has spatial directivity, and (t, μ, f) are the three-dimensional coordinates (τ is the space optical distance between a certain point and the incident light plane, μ is the angle between the emitted light and the vertical Z axis, and φ is the angle between the emitted light and the horizontal plane).

S represents the multi-scattering effect of the smoke particles in the smoke environment, which can be expressed by Eq. (5) [32]:

$$S(\tau, \mu, \varphi) = \frac{\omega}{4\pi} \int_0^{2\pi} d\varphi' \int_{-1}^1 d\mu' P(\tau, \mu, \varphi; \mu', \varphi') \times I(\tau, \mu', \varphi') \quad (5)$$

where P is the phase function, describing the probability of light scattering from the μ', φ' direction to the (μ, φ) direction. The Henyey Greenstein phase function can be used to simplify the calculation, as shown in Eq. (6) [32]:

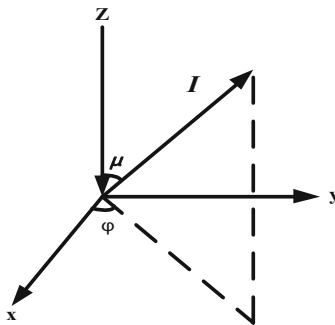


Figure 2. Space coordinate diagram of the radiative transfer equation.

$$P(\mu, \varphi; \mu', \varphi') = \frac{\omega}{4\pi} \times \frac{1 - g^2}{(1 + g^2 - 2g \cos \mu, \varphi; \mu', \varphi')} \quad (6)$$

In this equation, g is the asymmetry factor, which represents the symmetry between the forward and backward scattering of particles. ω is the single scattering reflectance, which represents the particle scattering ability and can be expressed by the ratio of the scattering ability to the total extinction ability, as shown in Eq. (7) [32]:

$$\omega = \frac{C_{\text{sca}}}{C_{\text{ext}}} \quad (7)$$

where C_{sca} is the scattering cross section of the smoke particles, and C_{ext} is the extinction cross section of the smoke particles, which represents the total attenuation of absorption and scattering. The optical thickness τ of the smoke layer can be expressed by Eq. (8) [32], which is used to describe the attenuation ability of the smoke layer:

$$\tau = \rho_n C_{\text{ext}} L \quad (8)$$

Here, ρ_n is the number concentration of the smoke particles, C_{ext} is the extinction section of the smoke particles, and L is the physical thickness of the smoke environment.

The transmission attenuation parameter for a single smoke particle is determined by the parameters of the radiative transfer equation (single scattering reflectance, asymmetry factor, and attenuation factor). The discrete ordinate method (DOM) is used to solve the radiative transfer equation [33]. Specifically, the DOM algorithm related software DISORT is used. The DOM method employs the Legendre polynomials to discretely expand the phase function in Eq. (6), then converts the integral operation in Eq. (5) into a differential form, and finally determines the transmission solutions in different directions through boundary conditions.

2.2. Experimental Design and Methods

The entire experimental flame area is separated from the flue gas area. The fire source is placed in the ignition furnace, and the flue gas collection box is placed on the optical platform. The terahertz detection equipment and the optical smoke density measurement equipment are placed on both sides of the experiment box. Figure 3 shows the diagram of the optical platform. The optical platform and the ignition furnace are connected by an aluminum foil hose, and a fan is connected between the two, which is used to pump the flue gas generated in the ignition furnace into the flue gas test box.

The terahertz detector is a passive imaging device. The center frequency of the terahertz wave emitted by the emission source is 0.1 THz, and the spectrum range collected by the receiving camera is about 50 GHz–700 GHz. As shown in Fig. 4,

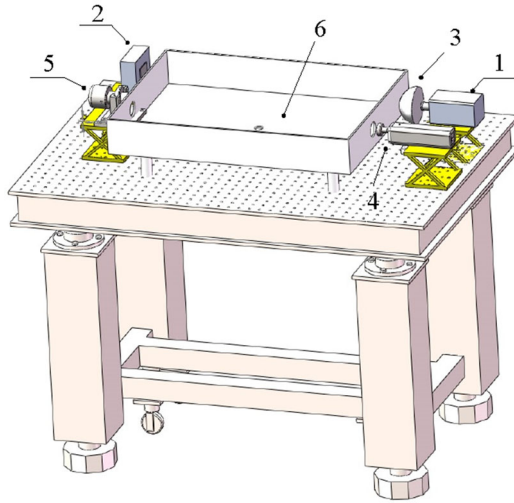


Figure 3. Optical experiment platform. 1 Terahertz wave emission source, 2 Terahertz camera, 3 Optical lens, 4 HeNe laser transmitter, 5 Silicon detector; 6 Flue gas experiment box.

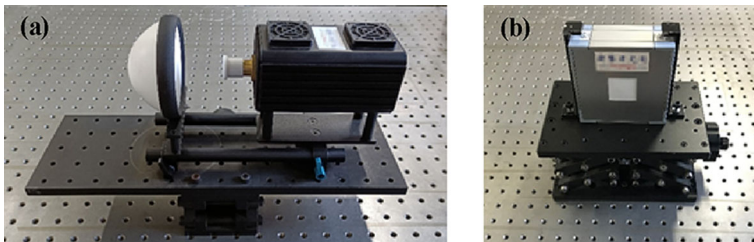


Figure 4. a Terahertz wave transmitting source equipment and b Terahertz camera.

the optical lens is installed in front of the terahertz wave transmitter to amplify the intensity of the transmitted terahertz wave, in order to improve the camera reception. A HeNe laser with a dominant wavelength of 632.8 nm and a silicon detector with a detection range of 350 nm–1100 nm are used to measure the smoke density. The flue gas environment is enclosed within a $700 \times 500 \times 100 \text{ mm}^3$ acrylic transparent box with a thickness of 5 mm. The box is supported by four solid transparent glass rods. A smoke inlet with a radius of 13 mm is located at the bottom of the box. The shorter side of the box has a circular hole with a radius of 21 mm, which corresponds to the size of the detection head of the optical smoke density measurement device, the circular hole improving the detection accuracy, avoid the influence of acrylic transparent box on terahertz waves imaging.

According to the GB4715-2005 standard experimental fire specifications, cotton rope smoldering fire, n-heptane open flame, and polyurethane open flame are selected as experimental fires. The three experimental fire sources are all placed in the ignition furnace when they are ignited, and a heat shield is placed at the bottom of the fire source for safety. When conducting a cotton rope smoldering fire experiment, the cotton rope is directly ignited and then quickly extinguished, with the pyrolysis stage being avoided.

The experiment is divided into three phases: preparation, combustion, and combustion end phase. Each group of experiments was recorded for 16 min, which can be subdivided into the preparation phase (60 s), combustion phase (600 s), and final phase during which the recording continued for 300 s after the combustion. Multiple sets of experiments were carried out for each standard experimental fire to verify the reliability of the experiment.

2.3. Working Conditions

Table 1 shows the amount of ignition material and experimental method used. The physical thickness of the flue gas layer corresponds to the size of the experimental smoke box, which is 0.7 m.

The particle size and concentration for the three fire smoke environments were measured with a scanning electromigration particle spectrometer and an ion smoke densitometer. The influence of the distance between the ignition area and the smoke test box, ambient temperature, and fan on the flue gas transmission rate was considered. Three standard experimental fires with an effective radius a_{eff} and a particle concentration ρ_n of the smoke particles at the five moments of ignition were used in the simulation. The time interval for each set of data selection is 2 min, corresponding to 120 s, 240 s, 360 s, 480 s and 600 s after ignition, so that

Table 1
Standard Fire Reference Table

Material (burning state)	Dosage	Experimental method
Cotton rope (smoldering)	50 pieces of clean and dry cotton ropes with a length of 50 cm	The cotton rope is evenly fixed on a metal ring with a diameter of 10 cm, and the ring is fixed on the bracket so that the cotton rope is suspended in air
N-heptane (open flame)	200 ml of n-heptane (purity $\geq 98.5\%$) liquid	The n-heptane liquid is poured into a square oil pan with a side length of 10 cm
Polyurethane (open flame)	3 pieces with dimensions of 30 cm (length) \times 10 cm (width) \times 4 cm (thickness) polyurethane plastic blocks	The 3 blocks are placed together in a square oil pan with a side length of 20 cm. The polyurethane block is placed on the edge of the oil pan and soaked in alcohol to facilitate ignition

the data selection covers the entire combustion process. The specific parameters are shown in Table 2.

The simulation data selection also takes into account the effects of turbulent condensation and Brownian condensation. The former primarily appears in the area near the flame during the combustion process, and the floating fire plume is formed by the combustion entrained air. The particle size gradually increases with the change in the air temperature and air velocity. The latter mainly occurs in the area of the flue gas layer and is also affected by turbulent condensation. In addition, after taking the generation rate of the combustion particles and the temperature changes into account, the Brownian condensation will change.

The actual fire environment is extremely complex and the simulation of the smoke characteristics in the experimental environment is not sufficient to establish an effective transmission model. When performing numerical simulation analyses, in addition to the verification of the experimental conditions, it is required to simulate and analyze the flue gas parameters in a comprehensive fire environment, and vary the terahertz wave wavelengths in order to analyze the influence of the change in wavelength on the transmission. The particle size D has values of 0.2 μm , 0.3 μm , 0.4 μm , 0.5 μm , 0.6 μm , 0.7 μm , and 0.8 μm . The effective radius $a_{eff} = D/2$ is used in the simulation. The particle number density ρ_n can take four values, namely 0.6×10^7 particles/ cm^3 , 0.9×10^7 particles/ cm^3 , 1.2×10^7 particles/ cm^3 , and 1.5×10^7 particles/ cm^3 , and the physical thickness of the smoke layer is set to 1 m. The terahertz wave is in the wavelength range of 31.25 μm –55.55 μm . As shown in Table 3, the complex refractive index of the terahertz wave is obtained from the HITRAN database and is the input parameter of the simulation [34].

3. Results and Analysis

3.1. Optical Smoke Density Measurement Result

When smoke particles enter the experiment box, the intensity of the light emitted by the optical transmitter is weakened after passing through the smoke layer. Therefore, the light intensity received by the receiver is reduced compared with the

Table 2
Three Standard Experimental Fire Smoke Particle Size and Concentration

Experimental fire type	Effective radius a_{eff} (μm)	Particle concentration ρ_n (particles/ cm^3)
N-heptane open flame	0.1/0.12/0.13/0.14/0.15	0.5/0.8/1.1/1.2/ 1×10^7
Polyurethane open flame	0.08/0.1/0.12/0.13/0.14	0.15/0.4/0.8/0.9/ 0.8×10^7
Cotton rope smoldering	0.06/0.08/0.1/0.12/0.13	0.2/0.45/0.63/0.64/ 0.65×10^7

Table 3
THz Waves Corresponding to the Complex Refractive Index in Smoke Particle

	Wavelength	Complex refractive index	
	$\lambda/\mu\text{m}$	n	k
1	31.25	2.583	0.342
2	33.33	2.597	0.336
3	35.71	2.612	0.334
4	38.46	2.631	0.334
5	41.66	2.66	0.333
6	45.45	2.697	0.323
7	50.00	2.731	0.295
8	55.55	2.754	0.264

initial light intensity, and the attenuation degree of the light has a functional relationship with the smoke concentration, which can be expressed by Eq. (9) [35]:

$$k = \frac{1}{L} \ln \left(\frac{I_0}{I} \right) \quad (9)$$

In this equation, k is the extinction coefficient (1/m); L is the physical thickness of the smoke layer(m); I_0 and I respectively represent the initial light intensity and real-time light intensity, which is given by the voltage (v). In order to facilitate comparisons, the initial light intensity of each experiment was modulated to $2v$.

Figure 5 shows the extinction coefficient k of the three standard experimental fires measured with the optical smoke density equipment during the experiment. The ignition time and extinguishing time are marked. It can be seen that when the combustion conditions are similar, the extinction coefficient of each standard fire is consistent across multiple experiments, and the rise rate and size change are almost constant. The error of the n-heptane open flame experiment curve is analyzed and found to have, a significant difference in the extinction coefficient curve between the two experiments. The curve representing the mean of the extinction coefficient curves of the two experiments is shown in the figure with a dotted line. The standard error σ varies between 0.0002 and 0.4 with an average value of 0.09. This indicates that the extinction curves obtained from the two experiments do not differ significantly, thus verifying the reliability of the experimental results.

By contrast, the extinction coefficient curves of the three standard fires show different sizes and rates of change. The rising rate of the n-heptane open flame is found to be the highest. Since it is directly ignited in the oil pan when it burns, it can fully combust, and the flue gas changes rapidly. The second fastest is the polyurethane foam open flame. Since it only ignites the accumulation of foam, the corner of the block does not maximize its combustion state instantaneously, and the rate of increase of the extinction coefficient is below that of the n-heptane

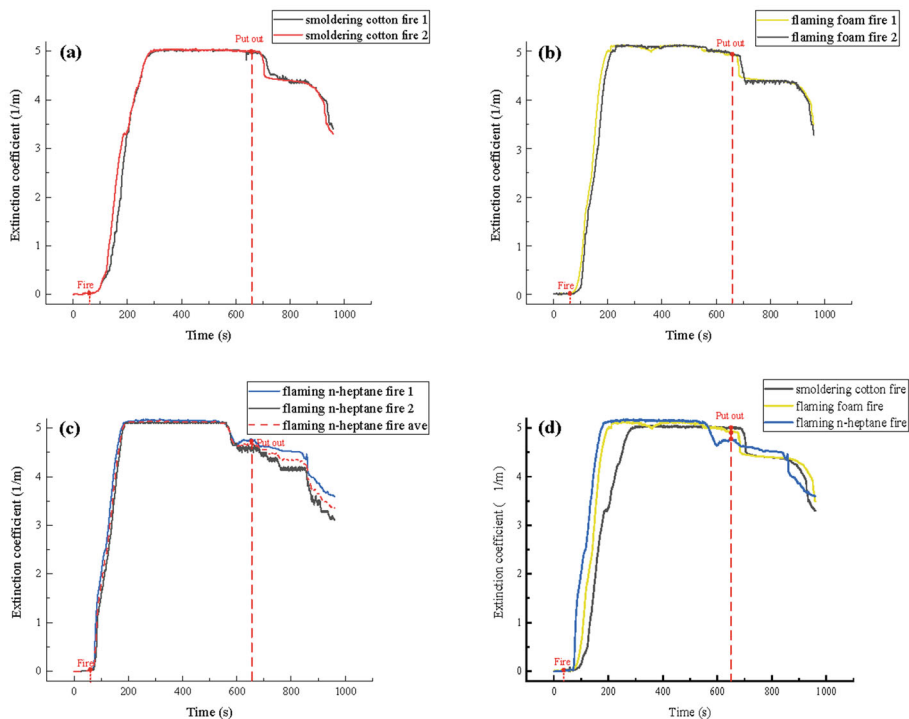


Figure 5. Time-sharing extinction coefficient measured with the optical smoke density equipment: a Cotton rope smolders, b polyurethane open flame, c n-heptane open flame, and d comparison of three types of standard fires.

open flame. The slowest change in the extinction coefficient is exhibited by the cotton rope smoldering fire. This is related to its burning state, and the rate at which the smoke particles are produced in the smoldering states is low. However, the smoke concentration in the flue gas test box can reach saturation within 4 min of ignition. The extinction coefficient of the n-heptane open flame experiment is the highest when it reaches a stable value, followed by those of the polyurethane foam open flame, and cotton rope smoldering open flame. The relationship between the extinction coefficients of the three standard fires is in agreement with their respective flue gas characteristics, which also confirms the appropriateness of the selection of the three standard fire parameters during the simulation.

After the burning material is extinguished, the extinction coefficients of the three standard fires decrease to varying degrees, and reach a constant state after a short period of decline. The n-heptane open flame is exhausted before the extinguishment of the fuel, so the extinction coefficient changes significantly before the extinguishing time, which is a normal phenomenon and does not affect the experimental results. The smoke exhaust system was turned on at 840 s to extract the

flue gas in the experiment box, and the extinction coefficient began to drop rapidly again until the end of the recording.

3.2. THz Equipment Test Results

The terahertz detection equipment adopts the detection method of video recording. The recording time corresponds to the optical smoke density detection. Each group of experiments intercepts the images of the terahertz detection system at four moments, which correspond to the images at 50 s, 200 s, 500 s and 800 s, covering the stage before ignition, initial flue gas stage, flue gas saturation stage, and combustion end stage.

The imaging standard is shown in Fig. 6. The color change represents the strength of the terahertz wave signal received by the terahertz receiving camera from the transmitter. Red represents complete reception, while blue and black represent complete occlusion. We quantify the received terahertz wave signal through the normalized “average”, “max”, and “min” values, and the value range of the three parameters is 0–1. “Average” represents the overall intensity of the terahertz wave signal received by the camera; “max” and “min” respectively represent the maximum and minimum values of the regional signal in the entire image.

The “average”, “max”, and “min” values before ignition in all experiments are all equal to 1, and the “max” value remains at 1 during the experiment. Figure 7a shows the corresponding images of the four moments detected by the terahertz equipment in the cotton rope smoldering experiment. At 200 s, the “average” value is $9.99\text{E}-01$, the “min” value is 0.996, and the image is unchanged. At 500 s, the “average” value is $9.93\text{E}-01$, the “min” value is 0.933, and a small part of the right edge of the image appears yellow. At 800 s, the “average” value is $9.98\text{E}-01$, the “min” value is 0.983, and the image shows no change. Overall, there is only a slight change in the image at around 500 s, and the transmittance of the terahertz wave can reach become greater than 99.3% during the entire

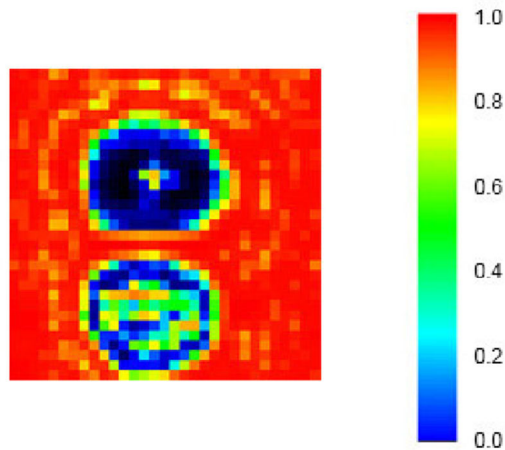


Figure 6. Terahertz equipment imaging standard.

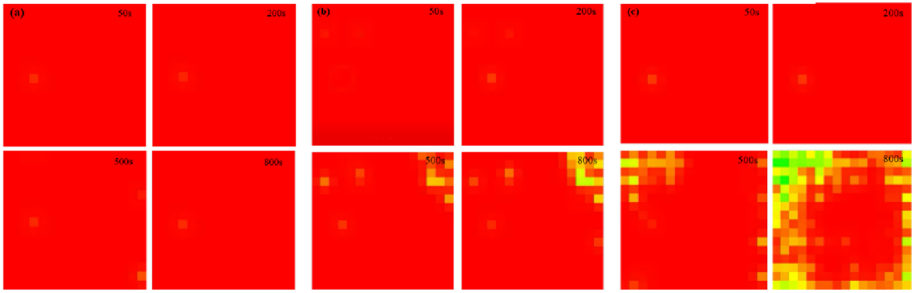


Figure 7. Terahertz detection images: a cotton rope smoldering image, b polyurethane open flame image, and c n-heptane open flame image.

experiment, indicating that the transmission of the terahertz wave is not affected by the smoke environment generated by the smoldering fire of the cotton rope.

Figure 7b shows the corresponding images of the four moments detected by the terahertz equipment in the polyurethane foam open flame experiment. At 200 s, the “average” value is $9.98\text{E}-01$, the “min” value is 0.994, and the image is unchanged. At 500 s, the “average” value is $9.88\text{E}-01$, the “min” value is 0.866, and a part of the upper right corner of the image appears yellow. At 800 s, the “average” value is $9.83\text{E}-01$, the “min” value is 0.733, and the upper right corner of the image becomes more yellow. According to the analysis, the yellow color of some areas of the image becomes darker at 800 s since polyurethane flame is a high polymer material, and the smoke particles are extremely sticky. After the combustion is completed, certain larger particles adhere to the side wall of the flue gas experiment box. Overall, the “min” value of the affected area reaches 0.733, which means that if the area is detected, the transmission transmittance of the terahertz wave can also reach 73% or more, and a good detection can thus be achieved. In the smoke environment generated by polyurethane, the “average” value of the entire received signal can be maintained above 0.98, indicating that the overall imaging detection can maintain a transmittance of above 98%.

Figure 7c shows the images of the four moments detected by the terahertz equipment in the n-heptane open flame experiment. At 200 s, the “average” value is $9.99\text{E}-01$, the “min” value is 0.986, and the image is unchanged. At 500 s, the “average” value is $9.84\text{E}-01$, the “min” value is 0.745, and yellow appears in the edge area of the image. At 800 s, the “average” value is $8.87\text{E}-01$, the “min” value is 0.533, and there is no discernible change in the center area of the image, but the edge shows a yellow green color. During the entire experiment, water vapor starts to appear 5 min after ignition. As the experiment progresses, the mixture of smoke particles and water vapor adheres to the inner wall of the experiment box. Therefore, the change in the image at 800 s is caused by the mixture of smoke particles and water droplets adhering to the inner wall of the experiment box. As the smoke concentration of the experiment box increases, some areas at the edge of the image appear yellow, indicating that the smoke environment generated by the n-heptane flame affects the terahertz wave imaging. Overall, the

transmission of terahertz waves is greatly affected by water vapor. Without the influence of water vapor, the transmission rate of terahertz waves in the n-heptane fire gas experiment can reach more than 98%. Under the influence of water vapor, the transmittance remains constant at about 90%.

Figure 8 shows the simulation results for the smoke environment generated by the three standard fires. The abscissa in the figure is the smoke particle size, the ordinate on the left is the particle concentration, and the ordinate on the right is the light transmittance. The upper curve in the figure corresponds to the transmittance of terahertz waves, and the lower curve corresponds to the smoke particle concentration. The simulation results show that the transmission transmittance of terahertz waves in cotton rope smoldering fires can exceed 99%, while the transmission transmittances in polyurethane open flames and n-heptane open flames can exceed 98%. The transmission of terahertz waves is affected by the changes in the flue gas and decreases as the size and concentration of the smoke particles increase.

Figure 9 shows the “min” value of the terahertz wave detection corresponding to the extinction coefficient detected by the optical smoke density measurement

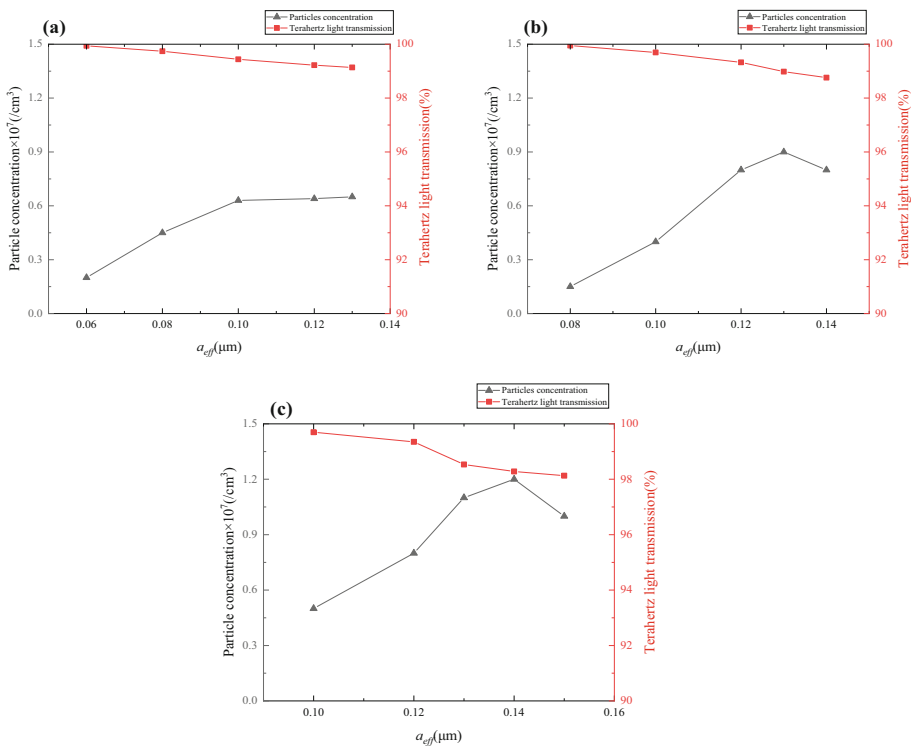


Figure 8. Simulation results for the three standard fire smoke environments: a cotton rope smoldering simulation, b polyurethane open flame simulation, and c n-heptane open flame simulation.

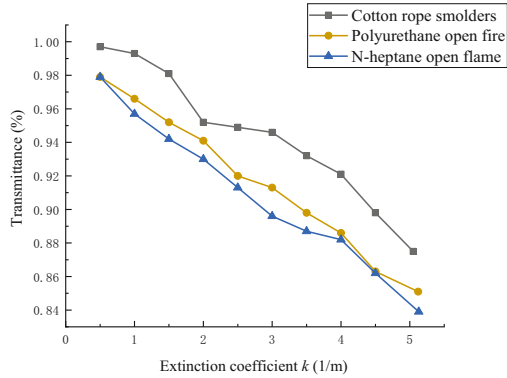


Figure 9. Terahertz wave transmittance corresponding to the extinction coefficient.

equipment. The “min” value of each standard fire is the average value obtained from two experimental records. The abscissa shows the stages of the change in the extinction coefficient in the initial stage of the standard fire experiments. In this way, the influence of the changing flue gas environment can be observed and analyzed. Two experimental datasets for the n-heptane open flame are used for standard error analysis. The range of the standard error σ of the two experiments is found to be less than 10^{-2} , which confirms the reliability of the transmittance measurement. From the figure, we can see that as the extinction coefficient increases, the “min” value begins to decrease. Among the three standard fire experiments, the transmission and permeability of terahertz waves in the cotton rope smoldering fire experiment are the best, while the transmission and permeability of terahertz waves in the n-heptane open flame experiment are the least but still relatively high. For regional imaging detection, in the three standard fire experiments, the minimum value of the terahertz wave signal collected by the camera can exceed 80%.

3.3. Simulation Results and Analysis

In order to establish an improved terahertz wave transmission model in a fire environment, a wide range of smoke particle sizes and particle concentrations is selected for the simulation analysis, and terahertz waves with different wavelengths are chosen for comparison. Considering the uncertainty in the incident direction of the terahertz wave and the change in the characteristics of the smoke particles, in this work, the smoke particles are rotated multiple times, and the average value is calculated when determining the attenuation characteristics.

Terahertz waves exhibit different attenuation characteristics for different smoke particle sizes, and different incident wavelengths also result in a varying attenuation. Figure 10 shows the light transmittance of the terahertz wave in the smoke particle group obtained via the radiative transmission equation. It can be seen from the figure that the transmission of the terahertz wave in the smoke environ-

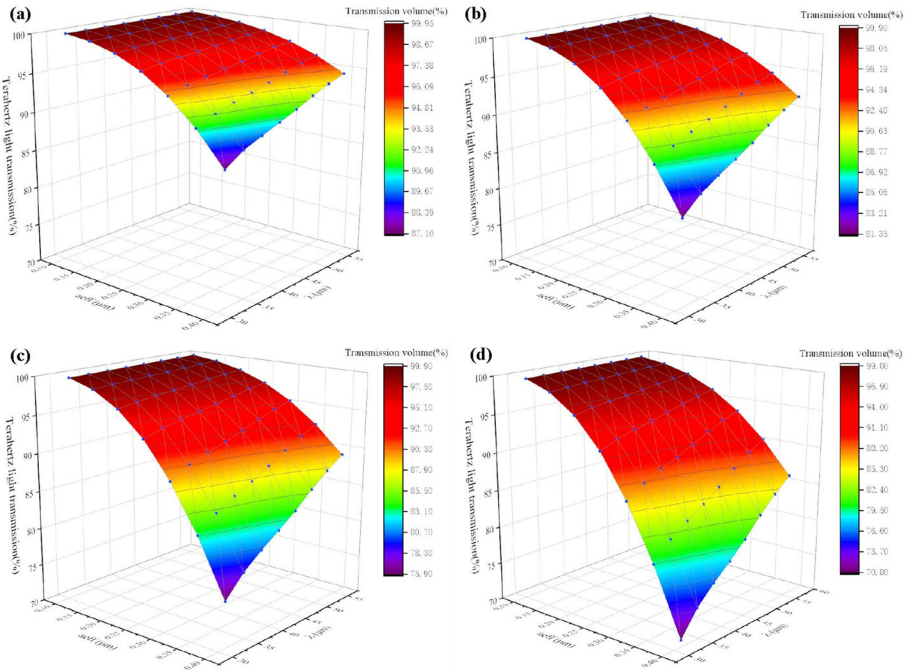


Figure 10. Influence of the incident light wavelength and particle size distribution on the light transmission **a** $\rho_n = 0.6 \times 10^7$ particles/cm³, **b** $\rho_n = 0.9 \times 10^7$ particles/cm³, **c** $\rho_n = 1.2 \times 10^7$ particles/cm³, and **d** $\rho_n = 1.5 \times 10^7$ particles/cm³.

ment decreases with the increase in the smoke particle size and increases with the increase in the wavelength of the incident wave. The light transmission also decreases as the smoke particle concentration increases. For high particle concentrations in the flue gas, the transmission is greatly affected by the particle size. If the particle size and concentration are low, the transmission of terahertz waves is almost unaffected. It is notable that terahertz waves can reach a transmittance of more than 70% in an environment with high particle concentration and large particle size.

4. Conclusion

In this work, the transmission characteristics of terahertz waves in the smoke environment generated by a fire were investigated. Passive terahertz imaging equipment was used to image and detect the smoke environment generated by three standard fires. An optical smoke density measuring instrument was used to detect real-time smoke density changes, in order to study the changes in terahertz imaging under different flue gas concentrations. The radiation transmission equation was used in the simulations. The influence of the size and concentration of

smoke particles on the transmission of terahertz waves with different wavelengths was analyzed via numerical simulations. A transmission model for terahertz waves in fire and smoke environments was established. It was experimentally found that in the early stage of the smoke environment generated by the fire (200 s before the experimental record), the smoke particles are small, their concentration is low, and the terahertz wave imaging is hardly affected by the smoke change. The terahertz wave emitted by the device could reach a fully transparent state, which can facilitate rescue in the initial moments of the fire. In the middle stage of the fire smoke environment (experimental record: 200 s–500 s), the smoke environment slowly developed from small particles at a low concentration to large particles at a high concentration and finally became saturated. Excluding the interference of other factors, the transmittance of terahertz waves in the flue gas environment at this stage could exceed 98%. In the middle and late stages of the fire (experimental record: 500–800 s), as the fuel burned out, the flue gas concentration started to decrease. Considering the interference of numerous factors (water vapor, condensed particulate matter, etc.), the transmittance of terahertz waves in the flue gas environment generated by a standard fire could be maintained above 80%. Overall, terahertz imaging in fire and smoke environments is significantly better than traditional detection techniques, and it can be beneficial for improving the imaging detection in low-visibility fire environments.

A real fire smoke environment is complex and changeable. Considering that the experimental environment is relatively simple, in addition to the analysis of the experimental conditions during the simulation analysis, a smoke environment with different smoke particle sizes and particle concentrations was also investigated. The simulation results showed that the attenuation characteristics of smoke particles to terahertz waves (single scattering reflectance, asymmetry factor, and extinction cross section) increase with the increase of the particle size of the smoke particles and decrease with the increase in the wavelength of the terahertz waves. In a flue gas environment, the terahertz waves were also found to be affected by the particle size distribution, and the transmission decreased with the increase in the particle size and concentration. However, it increased with the increase in the wavelength.

If the terahertz imaging detection technology will be used for the imaging detection of fire environments in the future, it will be necessary to fully consider the transmission characteristics of terahertz waves in fire and smoke environments. The research in this work is relatively limited, and experimental fires are too simple to simulate a real complex fire scene. For instance, the existence of many polymer composite materials in real fire environments could affect the terahertz imaging. Furthermore, the fact that metallic objects cannot pass through and hinder the imaging as well as the inevitable influence of water vapor in high-temperature environments must be taken into account. The terahertz imaging equipment used in this field also has certain limitations. The imaging area is small, which limits its application in fire and smoke environments. In future experiments, a terahertz array experimental platform will be built to conduct large-scale and human imaging experiments to improve the experimental data on fire and smoke environments, thereby yielding more comprehensive experimental results.

Acknowledgements

This work was supported by the National Natural Science Foundation for Young Scientists of China (51804278), the Science and Technology Research Project of the Henan Province (212102310385), and the Research Fund of the Zhengzhou University of Light Industry (2014BSJJ021).

Open Access

This article is licensed under a Creative Commons Attribution 4.0 International License, which permits use, sharing, adaptation, distribution and reproduction in any medium or format, as long as you give appropriate credit to the original author(s) and the source, provide a link to the Creative Commons licence, and indicate if changes were made. The images or other third party material in this article are included in the article's Creative Commons licence, unless indicated otherwise in a credit line to the material. If material is not included in the article's Creative Commons licence and your intended use is not permitted by statutory regulation or exceeds the permitted use, you will need to obtain permission directly from the copyright holder. To view a copy of this licence, visit <http://creativecommons.org/licenses/by/4.0/>.

References

1. Li P, Zhao WD (2020) Image fire detection algorithms based on convolutional neural networks. *Case Stud Thermal Eng.* 19:100625
2. Mitsunori A, Yunki T, Naofumi S (2019) Terahertz spectroscopy of CO and NO: The first step toward temperature and concentration detection for combustion gases in fire environments. *J Mol Spectrosc* 361:34–39
3. Zhang QX, Lin GH, Zhang YM et al (2018) Wildland Forest Fire Smoke Detection Based on Faster R-CNN using Synthetic Smoke Images. *Procedia Eng* 211:441–446
4. Siva M, Deep G (2018) Nonsubsampled contourlet domain visible and infrared image fusion framework for fire detection using pulse coupled neural network and spatial fuzzy clustering. *Fire Saf J* 101:84–101
5. Mao WT, Wang WP, Dou Z et al (2018) Fire recognition based on multi-channel convolutional neural network. *Fire Technol* 54(2):531–554
6. Frederico BC, Miguel AM, Pedro V et al (2021) Continuous wave terahertz imaging for NDT: Fundamentals and experimental validation. *Measurement* 172:108904
7. Li DD, Yang ZB, Fu AL et al (2020) Detecting melanoma with a terahertz spectroscopy imaging technique. *Spectrochim Acta Part A* 234:118229
8. Yang X, Wu T, Zhang L et al (2019) CNN with spatio-temporal information for fast suspicious object detection and recognition in THz security images. *Signal Process* 160:202–214
9. Leili AH, Elnaz A, Arash T et al (2020) Terahertz spectroscopy and imaging: A review on agricultural applications. *Comput Electron Agric* 177:105628
10. Li S, Feng CY, Liang XG et al (2018) A guided vehicle under fire conditions based on a modified ultrasonic obstacle avoidance technology. *Sensors* 18(12):4366

11. Zhang XB, Liu C, Zhang XY (2020) Quantitative observation of attenuation coefficient of electromagnetic wave propagation in haze incorporating charged aerosol. *J Quant Spectrosc Radiat Transfer* 257:107365
12. Medhurst RG (1965) Rainfall attenuation of centimeter waves: comparison of theory and measurement. *Trans Antennas Propag Mag* 13(4):550–564
13. Kahnert M (2016) Numerical solutions of the macroscopic Maxwell equations for scattering by non-spherical particles: a tutorial review. *J Quant Spectrosc Radiat Transfer* 178:22–37
14. Shen J, Cao NW, Yang SP et al (2020) Inversion of aerosol extinction coefficient by Raman-Mie scattering lidar. *Optik* 203:164038
15. Dong QF, Guo LX, Li Y et al (2017) Weathering Sand and Dust Storms: Particle shapes, storm height, and elevation angle sensitivity for microwave propagation in earth-satellite links. *IEEE Antennas Propag Mag* 59(1):58–65
16. Zhao XY, Hu YH, Gu YL et al (2019) A comparison of infrared extinction performances of bioaerosols and traditional smoke materials. *Optik* 181:293–300
17. Zhang YG, Tian AL, Liu BC et al (2019) Stokes parameters polarization scattering properties of optical elements surface of different material. *Optik* 185:1238–1246
18. Li HY, Wu ZS, Bai L et al (2014) Scattering and propagation of terahertz pulses in random soot aggregate systems. *Chin Phys B* 23(5):054201
19. Wang QC, Wang JC, Zhao DP et al (2015) Study on the transmission ability of terahertz wave through smoke screen. *Infrared Laser Eng* 44(12):3696–3700
20. Ken M, Naofumi S, Seiji O (2017) Advanced active imaging system for fires based on terahertz electromagnetic waves: Experimental study of effectiveness in smoky and high-temperature environments. *Fire Saf J* 91:1051–1058
21. Qiao LF, Zhang YM, Xie QY (2007) Fractal structure shape simulation and light scattering calculation of fire smoke particles. *Acta Physica Sinica* 56(11):6736–6741
22. Zhang Q, Deng XJ, Zhang QX et al (2010) Comparative study of light scattering between the fractal model of fire smoke particles and the spherical model. *Acta Physica Sinica* 59(10):7442–7446
23. Zurita M, Rosner DE (2002) Effective diameters for collisions of fractal-like aggregates: recommendations for improved aerosol coagulation frequency predictions. *J Colloid Interface Sci* 255(1):10–26
24. Mishchenko MI, Liu L, Travis LD et al (2004) Scattering and radiative properties of semi-external versus external mixtures of different aerosol types. *J Quant Spectrosc Radiat Transfer* 88(1):139–147
25. Liu J, Zhang QX, Huo YN et al (2020) An experimental study on light scattering matrices for Chinese loess dust with different particle size distributions. *Atmos Measur Tech* 13(8):4097–4109
26. Draine BT (1988) The discrete-dipole approximation and its application to interstellar graphite grains. *Astrophys J* 333:848–872
27. Xie T, Chen MT, Chen J et al (2020) Scattering and absorption characteristics of non-spherical cirrus cloud ice crystal particles in terahertz frequency band. *Chin Phys B* 29(7):145–152
28. Draine BT, Flatau PJ (2013) New York(NY): User guide for the discrete dipole approximation code DDSCAT 7.3. Available from: <https://arxiv.org/abs/1305.6497>. Accessed 26 May 2013
29. Goodman JJ, Draine BT, Flatau PJ (2002) Application of fast-Fourier-transform techniques to the discrete-dipole approximation. *Opt Lett* 255(1):10–26
30. Tam WG, Zardecki A (1982) Multiple scattering corrections to the Beer-Lambert law I: open detector. *Appl Opt* 21(13):2405–2412

31. Zardecki A, Tam WG (1982) Multiple scattering corrections to the Beer-Lambert law. 2: detector with a variable field of view. *Appl Opt* 21(13):2413–2420
32. Knut S, Tsay SC, Wiscombe W, Jayaweera K (1988) Numerically stable algorithm for discrete-ordinate-method radiative transfer in multiple scattering and emitting layered media. *Appl Opt* 27(12):2502–2509
33. Kang SH, Song TH (2008) Finite element formulation of the first- and second-order discrete ordinates equations for radiative heat transfer calculation in three-dimensional participating media. *J Quant Spectrosc Radiat Transfer* 109(11):2094–2107
34. Polyanskiy MN. Refractive index database. Available from: <https://refractiveindex.info>
35. Joseph WS, Lattimer BY (2014) Evaluation of navigation sensors in fire smoke environments. *Fire Technol* 50(6):1459–1481

Publisher's Note Springer Nature remains neutral with regard to jurisdictional claims in published maps and institutional affiliations.